PNAS RESEARCH ARTICLE | APPLIED PHYSICAL SCIENCES

Skin effect as a probe of transport regimes in Weyl semimetals

Paweł Matus[a,b], Renato M. A. Dantas[a,b,c], Roderich Moessner[a,b], and Piotr Surówka[a,b,d,1]

Edited by Angel Rubio, Max-Planck-Institut fur Struktur und Dynamik der Materie, Hamburg, Germany; received January 8, 2022; accepted February 11, 2022

We study the propagation of an oscillatory electromagnetic field inside a Weyl semimetal. In conventional conductors, the motion of the charge carriers in the skin layer near the surface can be diffusive, ballistic, or hydrodynamic. We show that the presence of chiral anomalies, intrinsic to the massless Weyl particles, leads to a hitherto neglected nonlocal regime that can separate the normal and viscous skin effects. We propose to use this regime as a diagnostic of the presence of chiral anomalies in optical conductivity measurements. These results are obtained from a generalized kinetic theory that includes various relaxation mechanisms, allowing us to investigate different transport regimes of Weyl semimetals.

skin effect | Weyl semimetals | quantum anomalies

Significance

Weyl semimetals are a class of three-dimensional materials, whose low-energy excitations mimic massless fermions. In consequence they exhibit various unusual transport properties related to the presence of chiral anomalies, a subtle quantum phenomenon that denotes the breaking of the classical chiral symmetry by quantum fluctuations. In this work we present a universal description of transport in weakly disordered Weyl semimetals with several scattering mechanisms taken into account. Our work predicts the existence of a new anomaly-induced transport regime in these materials and gives a crisp experimental signature of a chiral anomaly in optical conductivity measurements. Finally, by also capturing the hydrodynamic regime of quasiparticles, our construction bridges the gap between developments in electronic fluid mechanics and three-dimensional semimetals.

Electronic transport phenomena often present particularly direct and accurate probes of the properties of conducting materials. Conventional metals are well described by the Drude theory that captures the diffusive movement of charge carriers. In very clean materials, where the scattering of electrons with impurities is not frequent, transport departs from being diffusive. Depending on the interaction strength, transport exhibits either ballistic or hydrodynamic behavior (1, 2). So far the experimental candidates to investigate such effects are two-dimensional (Al,Ga)As heterostructures (3–5) and graphene (6–12). A detailed theoretical analysis describing viscous electronics and ballistic-to-hydrodynamic cross-overs in clean two-dimensional structures is done by means of kinetic theory with various relaxation times corresponding to different scattering mechanisms (13, 14).

In a parallel line of developments, much effort has been devoted to the study of topological effects in the transport of massless quasiparticles. In three dimensions, these can be realized as low-energy electronic excitations in materials known as Dirac semimetals and Weyl semimetals. In Weyl semimetals either time-reversal symmetry or inversion symmetry is absent and the spectrum in the vicinity of the Fermi energy consists of an even number of linear band crossings known as Weyl nodes. Each crossing hosts fermions with a well-defined chirality, and the sum of the chiralities in the Brillouin zone is zero (15, 16). The fact that the Weyl nodes are generically separated in the reciprocal space makes these systems an ideal platform to investigate transport phenomena related to the chiral anomaly. It describes the breaking of the classical chiral symmetry by quantum fluctuations in parallel electric and magnetic fields (17–19). At weak coupling, the imprint of the chiral anomaly has been connected to negative magnetoresistance observed in Dirac and Weyl semimetals (20–28). In the hydrodynamic regime, macroscopic effects tied to chiral anomalies are the chiral magnetic effect (CME), the chiral vortical effect, and thermal transport phenomena related to gravitational anomalies (29–38). Despite the above predictions, on the one hand, the direct identification of the chiral anomalies with negative magnetoresistance is problematic due to other interfering effects (39); on the other hand, the hydrodynamic regime is more difficult to control experimentally (for recent progress see refs. 40 and 41) and the corresponding effects are difficult to measure in practice.

The relevant degrees of freedom to capture transport in semimetals with a finite Fermi energy and at low temperatures can be modeled as long-lived quasiparticles. In this case the pertinent quantity is the single-particle distribution function due to the fact that we can treat interactions perturbatively. The evolution of the single-particle distribution function is given by the Boltzmann kinetic equation, which incorporates both the single-particle dynamics and the relaxation processes arising from interactions between constituents of the system. This provides the semiclassical description of physical observables that vary slowly in space and time, establishing a statistical description of a many-body electron system. The effect of collisions of the particles has to be encapsulated by an appropriate choice of the collision term, which is usually done by a phenomenological treatment of the appropriate relaxation mechanisms (42, 43). In the case of massless fermions under the influence of an external magnetic field, the classical evolution gets modified due to the Berry phase contribution. Thus, the dynamics of the distribution function also change and are given by the chiral kinetic equation (44–48).

Author contributions: R.M. and P.S. designed research; P.M., R.M.A.D., and P.S. performed research; and P.M., R.M.A.D., and P.S. wrote the paper.

The authors declare no competing interest.

This article is a PNAS Direct Submission.

[1]To whom correspondence may be addressed. Email: surowka@pks.mpg.de.

This article contains supporting information online at https://www.pnas.org/lookup/suppl/doi:10.1073/pnas.2200367119/-/DCSupplemental.

Published March 14, 2022.

Transport properties of Weyl semimetals are not limited to steady flow configurations. In fact, semimetals driven by alternating current (ac) electric fields exhibit a rich phenomenology and reveal new effects absent in direct current (dc) settings in both two (49–57) and three dimensions (58–67).

Here, our goal is to investigate the ramifications of chiral anomalies on transport properties at finite frequency. One of the classic examples of a finite driving transport phenomenon is the skin effect (68). It states that an alternating electric current is distributed mainly close to the wall of the conductor and decays exponentially within the conductor. Therefore, the skin effect increases its effective resistance through the reduction of the effective cross-section of the conductor. This reduction is parameterized by a distance, called the penetration depth or the skin depth, that depends on the driving frequency. Depending on the dominant relaxation mechanism in the skin layer, which in general changes with the skin depth, three types of skin effect are conventionally distinguished: normal, anomalous, and viscous (2, 69). The normal skin effect assumes that the constitutive relation between the current and the electric field is local. The anomalous skin effect appears when this assumption is not valid and the local current depends nonlocally on the field distribution. Note that the name anomalous skin effect should not be confused with the influence of chiral anomalies. Both the normal and anomalous skin effects appear when the interactions between electrons are weak. Third, the viscous skin effect manifests itself in clean materials when the interactions between charge carriers become large and the charge flow is described by hydrodynamics. It is an example of boundary layer phenomena in fluid mechanics that arise in the immediate vicinity of a bounding surface where the effects of viscosity are significant.

The goal of this paper is to study skin effects for a Weyl metal, focusing on imprints of chiral anomalies. Chiral anomaly leads to the appearance of the chiral magnetic current (23)

$$\mathbf{J}_{\mathrm{CME}} \propto \tau_5 (\mathbf{E}\cdot\mathbf{B})\mathbf{B}, \qquad [1]$$

where τ_5 is the time needed for the relaxation of the axial charge (i.e., the difference between the charge densities of the particles with opposite chirality). In the standard treatment, which focuses on the dc conductivity, τ_5 is related to internode scattering induced by impurities (70–72). However, when an ac field is applied, different relaxation mechanisms may become dominant.

In this work we provide a detailed study of the change of the chiral magnetic conductivity across a wide frequency spectrum. To this end, we generalize the chiral kinetic theory framework to account for different relaxation processes present in realistic materials. These processes include momentum-relaxing collisions coming from the scattering of quasiparticles with impurities as well as momentum-conserving collisions between quasiparticles. We follow the path of expanding the collision kernel in the eigenfunctions of the angular momentum. Such a procedure was successfully applied in the context of two-dimensional materials (73–77).

In the process we uncover a transport regime, the existence of which depends on the presence of the chiral anomaly. In this regime the relaxation of momentum is dominated by scattering off impurities, but the relaxation of the axial charge in the skin layer takes place mainly through the diffusion of particles out of the layer and into the bulk of the material. This process causes a significant increase of the skin depth, as well as a different scaling of the surface impedance with frequency, in the presence of magnetic field. This observation gives a clear experimental imprint of the chiral anomalies in optical conductivity measurements.

Transport Regimes and the Skin Effect

The skin effect is concerned with the flow of charge in a conductor under the influence of an oscillating electric field. It was first discovered in the context of spherical conductors (78) as a consequence of Maxwell's equations, which impose the propagation of electric field in a medium to be described by the equation

$$\nabla^2\mathbf{E} - \nabla(\nabla\cdot\mathbf{E}) - c^{-2}\partial_t^2\mathbf{E} = \mu\partial_t\mathbf{J}, \qquad [2]$$

where $\mathbf{J}$ is the current density, c is the speed of light, and μ is the magnetic permeability in the medium. When propagating inside a conductor, the electric field is attenuated by the induced currents and the magnitude of the field drops exponentially with the distance. This decay is characterized by a length δ called the skin depth (Fig. 1). To study the skin effect, one needs to supplement Maxwell's equations with a model describing the dynamics of particles in an electric field. The simplest model providing such dynamics is of the constitutive type and assumes a local relation between the current $\mathbf{J}(x,t)$ and the electric field $\mathbf{E}(x,t)$. This assumption is not always justified and nonlocal effects have to be taken into account, which can be done for almost free electrons by resorting to kinetic theory (79). Finally, in clean materials the relation between the current and the electric field can be hydrodynamic and controlled by the fluid viscosity. Kinetic theory can also be used to capture the effects of viscosity, providing a unified interpretation of various regimes in terms of different scattering mechanisms in the conductor, which affects the final form of the optical conductivity (80).

Electrons moving in the bulk of a (semi)metal experience different types of scattering: 1) electron–electron collisions, which conserve the total momentum, and 2) electron–impurity and electron–phonon collisions, which dissipate momentum. Correspondingly, we denote the mean free path between momentum-conserving collisions as l_{mc} and the mean free path for momentum-relaxing collisions as l_{mr}. Other length scales essential to the problem are the skin depth δ, as well as the path traversed by an electron over one period of oscillation of the field, $l_\omega \approx v_{\mathrm{F}}/\omega$, where v_{F} is the Fermi velocity and ω is the frequency of the driving electric field. Depending on the relative values of these length scales, one can distinguish the following different transport regimes:

1) When $l_{\mathrm{mr}} \ll \delta$ or $l_\omega \ll \delta$, the electric field can be assumed to be uniform on the length of the free path of an electron,

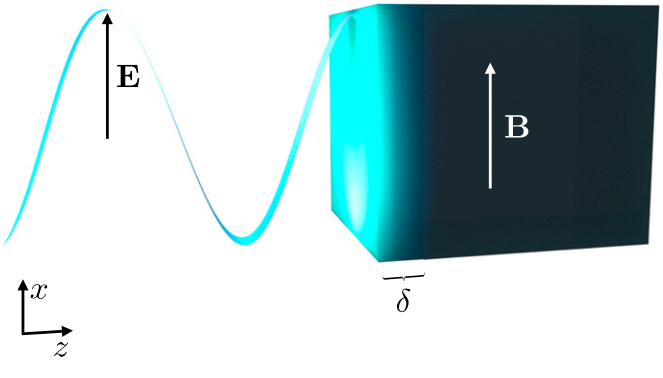

Fig. 1. A schematic illustration of the skin effect. The propagation of an electromagnetic wave entering a conductor is limited to a layer of width δ, called the skin depth. The skin depth changes with the frequency of the electric field ω, making it possible to probe different transport regimes in a single sample of a Weyl semimetal. To determine the effect of the chiral anomaly on transport, the sample is placed in an external magnetic field **B** aligned parallel to the propagating electric field.

and consequently the relation between the electric field and electric current is local in space: $\mathbf{J}(\mathbf{x},\omega)=\sigma(\omega)\mathbf{E}(\mathbf{x},\omega)$. This is the regime where the usual Drude formula for optical conductivity can be used. The skin effect in this regime is called the normal skin effect (78). In this article we further differentiate between the low-frequency normal regime (when l_{mr} is the shortest length scale) and the high-frequency normal regime (when l_ω is the shortest length scale).

2) In the case of very pure samples at low temperatures, the electron–impurity and electron–phonon collisions can become less frequent than the electron–electron collisions; that is, $l_{\mathrm{mc}}\ll l_{\mathrm{mr}}$. Then, in some frequency range it may happen that $l_{\mathrm{mc}}\ll\delta\ll l_{\mathrm{mr}}$. In that case, the motion of the electron can be seen as a random walk with step size equal to l_{mc}. The length of the path that an electron has to traverse to cross the skin layer is of the order δ^2/l_{mc}, so momentum relaxation in the skin layer happens on the length scale of $\min\{\delta^2/l_{\mathrm{mc}},l_{\mathrm{mr}}\}$. If the condition $\delta^2/l_{\mathrm{mc}}\ll l_{\mathrm{mr}}$ is fulfilled, we are in the hydrodynamic regime, where the skin effect is known as the viscous skin effect, first studied by Gurzhi (81).

3) Finally, when in some frequency range δ is the smallest length scale, i.e., $\delta\ll\min\{l_{\mathrm{mr}},l_{\mathrm{mc}},l_\omega\}$, we enter a regime in which electrons can be assumed not to undergo any scattering in the skin layer, so the motion of the electrons is ballistic. The skin effect in this regime is called the anomalous skin effect (79).

In Weyl metals the presence of the chiral anomaly complicates this picture. When the material is placed in parallel electric and magnetic fields, the axial anomaly causes an imbalance between the densities of quasiparticles with different chiralities, and the chiral magnetic effect gives rise to the current in Eq. **1**. Therefore, in addition to the rate of relaxation of momentum, also the rate of relaxation of the axial charge becomes relevant for the transport of electric charge.

While at low frequencies both momentum and axial charge relaxation originate in the same physical processes, namely collisions with impurities, the relevant length scale for the latter, which we call l_{inter}, can be much longer than l_{mr} (70–72). Consequently, in a certain frequency range $l_{\mathrm{mr}}\ll\delta\ll l_{\mathrm{inter}}$ can occur. In analogy to our discussion of the hydrodynamic regime, in addition to the internode scattering, relaxation of the axial charge takes place also through diffusion. Since $l_{\mathrm{mr}}\ll\delta$, we are in the diffusive regime and the time needed for the charge imbalance to diffuse through the skin layer is of the order $\delta^2/(v_{\mathrm{F}}l_{\mathrm{mr}})$. If the condition $\delta^2/l_{\mathrm{mr}}\ll l_{\mathrm{inter}}$ is satisfied, diffusion becomes the primary mechanism of the axial charge relaxation in place of the internode scattering. The characteristic feature of this regime is that while the classical contribution to the conductivity can still be described by the local Drude formula, the contribution resulting from the quantum anomaly is nonlocal. Therefore, we call this regime the anomaly-induced nonlocal (AIN) regime. The interplay between the classical and quantum contributions has nontrivial consequences for the skin effect.

Kinetic Theory with Second-Order Corrections

Our aim is to calculate currents in a Weyl semimetal by solving the Boltzmann kinetic equation. Hereafter, we consider a Weyl semimetal composed of two Weyl nodes with opposite chirality and assume that there are no other bands contributing to the conductivity. Consequently, we consider two distribution functions $f^{(s)}$ labeled by the chirality of the node $s=\pm1$. In the vicinity of the node with chirality s, and in the absence of external fields, we take the system to be described by the idealized low-energy Hamiltonian,

$$H(\mathbf{p})=sv\boldsymbol{\sigma}\cdot\mathbf{p}. \qquad [3]$$

For such a Hamiltonian, the dispersion relation for the conduction bands takes the simple form

$$\epsilon_0(\mathbf{p})=v|\mathbf{p}|. \qquad [4]$$

Finally, our semiclassical approach assumes a system whose Fermi energy ϵ_F satisfies the inequalities $kT\ll\epsilon_{\mathrm{F}}$ and $\hbar\omega\ll\epsilon_{\mathrm{F}}$, such that there are no antiparticle excitations.

The semiclassical equations of motion in the chiral kinetic theory are

$$D^{(s)}\dot{\mathbf{x}}^{(s)}=\left[\mathbf{v}_{\mathrm{M}}^{(s)}+e\hbar\mathbf{E}\times\boldsymbol{\Omega}^{(s)}+e\hbar\left(\mathbf{v}_{\mathrm{M}}^{(s)}\cdot\boldsymbol{\Omega}^{(s)}\right)\mathbf{B}\right], \qquad [5]$$

$$D^{(s)}\dot{\mathbf{p}}^{(s)}=\left[e\mathbf{E}+e\mathbf{v}_{\mathrm{M}}^{(s)}\times\mathbf{B}+e^2\hbar(\mathbf{E}\cdot\mathbf{B})\boldsymbol{\Omega}^{(s)}\right], \qquad [6]$$

where $\mathbf{v}_{\mathrm{M}}^{(s)}=\partial_{\mathbf{p}}\epsilon_{\mathrm{M}}^{(s)}$ is the group velocity and

$$D^{(s)}=1+e\hbar\mathbf{B}\cdot\boldsymbol{\Omega}^{(s)} \qquad [7]$$

is the volume element of the phase space in the presence of the Berry curvature $\boldsymbol{\Omega}^{(s)}$ (46, 82). Charge and current densities are defined as

$$\rho(\mathbf{x},t)=e\sum_{s=\pm1}\int\frac{d^3p}{(2\pi\hbar)^3}D^{(s)}f^{(s)}(\mathbf{x},\mathbf{p},t), \qquad [8]$$

$$\mathbf{J}(\mathbf{x},t)=e\sum_{s=\pm1}\int\frac{d^3p}{(2\pi\hbar)^3}D^{(s)}\dot{\mathbf{x}}^{(s)}f^{(s)}(\mathbf{x},\mathbf{p},t). \qquad [9]$$

The distribution functions $f^{(s)}(\mathbf{x},\mathbf{p},t)$ can be determined from the corresponding Boltzmann equations

$$\partial_t f^{(s)}+\dot{\mathbf{x}}^{(s)}\cdot\partial_{\mathbf{x}}f^{(s)}+\dot{\mathbf{p}}^{(s)}\cdot\partial_{\mathbf{p}}f^{(s)}=C^{(s)}[f^{(s)},f^{(-s)}], \qquad [10]$$

where $C^{(s)}$ is the collision integral (discussed in the next section).

The presence of external fields changes the simple dispersion relation given in Eq. **4**. In particular, corrections linear in $\mathbf{B}$, related to the orbital magnetic moment (OMM) of the wavepackets, have been shown to lead to a qualitative change in the magnetoconductance (83, 84). As the chiral magnetic effect is seen on the order $\mathbf{B}^2$, corrections to the semiclassical equations of motion quadratic in $\mathbf{B}$ can also potentially affect the result. For that reason, in this work we include second-order corrections to the energy (85) (*SI Appendix*):

$$\epsilon_{\mathrm{M}}^{(s)}(\mathbf{p})=v\left[|\mathbf{p}|-s\frac{e\hbar\mathbf{B}\cdot\mathbf{p}}{2|\mathbf{p}|^2}+\frac{e^2\hbar^2|\mathbf{B}|^2}{8|\mathbf{p}|^3}-\frac{e^2\hbar^2\left(\mathbf{B}\cdot\mathbf{p}\right)^2}{8|\mathbf{p}|^5}\right]. \qquad [11]$$

The magnetic field also modifies the Berry curvature (85, 86) (*SI Appendix*), which up to linear order in $\hbar$ reads

$$\boldsymbol{\Omega}^{(s)}(\mathbf{p})=s\frac{\mathbf{p}}{2|\mathbf{p}|^3}-\frac{e\hbar\mathbf{B}}{4|\mathbf{p}|^4}+\frac{e\hbar(\mathbf{B}\cdot\mathbf{p})\mathbf{p}}{2|\mathbf{p}|^6}. \qquad [12]$$

Using these formulas, the equations of motion are valid up to order $\mathbf{B}^2$. Second-order corrections to the equations of motion in the context of chiral kinetic theory were considered before in refs. 87–89.

It is important to state that the semiclassical approach is valid only for sufficiently weak magnetic fields. To be more precise, it is assumed that the dimensionless parameter

$$\alpha = \frac{e\hbar|\mathbf{B}|v^2}{2\epsilon_{\mathrm{F}}^2} \qquad [13]$$

satisfies $\alpha \ll 1$; otherwise the analysis would have to take into account the quantization of the Landau levels. Thus, α quantifies the magnitude of quantum corrections to the classical equations of motion.

Linearized Boltzmann Equation

The collision term $C^{(s)}[f^{(s)}, f^{(-s)}]$ in Eq. **10** is zero when both particle species follow the Fermi–Dirac distribution; i.e., $C^{(s)}[f_0^{(s)}, f_0^{(-s)}] = 0$ with

$$f_0^{(s)}(\mathbf{p}) = \left[\exp\left(\frac{\epsilon_{\mathrm{M}}^{(s)}(\mathbf{p}) - \epsilon_{\mathrm{F}}}{kT}\right) + 1\right]^{-1}. \qquad [14]$$

To solve the Boltzmann equation, $f^{(s)}$ is expanded around $f_0^{(s)}$. Setting $f^{(s)} = f_0^{(s)} + f_1^{(s)}$ in Eq. **10** shows that the leading-order solution f_0 contributes a term proportional to $\partial_{\mathbf{p}} f_0^{(s)} = \partial_{\mathbf{p}} \epsilon_{\mathrm{M}}^{(s)} \cdot \partial_{\epsilon_{\mathrm{M}}} f_0^{(s)}$ to the equation. Consequently, we parameterize the full solution as follows:

$$f^{(s)} = f_0^{(s)}(\mathbf{p}) + \partial_{\epsilon_{\mathrm{M}}} f_0^{(s)} \cdot \eta^{(s)}(\mathbf{x}, \mathbf{p}, t). \qquad [15]$$

For $kT \ll \epsilon_{\mathrm{F}}$, $\partial_{\epsilon_{\mathrm{M}}} f_0^{(s)} \approx -\delta\left[\epsilon_{\mathrm{M}}^{(s)}(\mathbf{p}) - \epsilon_{\mathrm{F}}\right]$, which means that we have only to pay attention to $\eta^{(s)}(\mathbf{x}, \mathbf{p}, t)$ with momenta $\mathbf{p}$ close to the Fermi surface. The shape of the Fermi surface is determined by equating the right-hand side (RHS) of Eq. **11** to ϵ_{F} and solving for $|\mathbf{p}|$. To that end, we introduce the unit vectors pointing in the direction of magnetic field and momentum,

$$\hat{\mathbf{b}} = \mathbf{B}/|\mathbf{B}|, \qquad \hat{\mathbf{p}} = \mathbf{p}/|\mathbf{p}|, \qquad [16]$$

respectively. The Fermi momentum in the direction $\hat{\mathbf{p}}$ can then be written, up to the second order in $\mathbf{B}$, as

$$p_{\mathrm{F}}^{(s)}(\hat{\mathbf{p}}) = \frac{\epsilon_{\mathrm{F}}}{v}\left[1 + s\alpha(\hat{\mathbf{p}}\cdot\hat{\mathbf{b}}) - \frac{1}{2}\alpha^2 - \frac{1}{2}\alpha^2(\hat{\mathbf{p}}\cdot\hat{\mathbf{b}})^2\right]. \qquad [17]$$

Using this result it is possible to evaluate the Berry curvature $\mathbf{\Omega}^{(s)}$ and the group velocity $\mathbf{v}_{\mathrm{M}}^{(s)}$ at the Fermi surface up to the second order in α:

$$\mathbf{\Omega}^{(s)}(p_{\mathrm{F}}^{(s)}(\hat{\mathbf{p}}), \hat{\mathbf{p}}) = \frac{1}{e\hbar|\mathbf{B}|}\left[s\alpha\hat{\mathbf{p}} - \alpha^2\hat{\mathbf{b}}\right], \qquad [18]$$

$$\mathbf{v}_{\mathrm{M}}^{(s)}(p_{\mathrm{F}}^{(s)}(\hat{\mathbf{p}}), \hat{\mathbf{p}}) = v\left[\hat{\mathbf{p}} - s\alpha\hat{\mathbf{b}} + 2s\alpha(\hat{\mathbf{p}}\cdot\hat{\mathbf{b}})\hat{\mathbf{p}} - \frac{3}{2}\alpha^2\hat{\mathbf{p}} + \alpha^2(\hat{\mathbf{p}}\cdot\hat{\mathbf{b}})\hat{\mathbf{b}} - \frac{3}{2}\alpha^2(\hat{\mathbf{p}}\cdot\hat{\mathbf{b}})^2\hat{\mathbf{p}}\right]. \qquad [19]$$

In what follows we make the dependence on p_{F} implicit; i.e., $\mathbf{\Omega}^{(s)}(p_{\mathrm{F}}^{(s)}(\hat{\mathbf{p}}), \hat{\mathbf{p}}) \equiv \mathbf{\Omega}^{(s)}(\hat{\mathbf{p}})$, $\mathbf{v}_{\mathrm{M}}^{(s)}(p_{\mathrm{F}}^{(s)}(\hat{\mathbf{p}}), \hat{\mathbf{p}}) \equiv \mathbf{v}_{\mathrm{M}}^{(s)}(\hat{\mathbf{p}})$, $\eta^{(s)}(p_{\mathrm{F}}^{(s)}(\hat{\mathbf{p}}), \hat{\mathbf{p}}) \equiv \eta^{(s)}(\hat{\mathbf{p}})$.

Next, we turn our attention to the collision term on the RHS of Eq. **10**. We linearize this term by introducing the collision operator $\hat{C}^{(s)}$ defined as

$$\hat{C}^{(s)}[\eta^{(s)}, \eta^{(-s)}] \equiv \left(\partial_{\epsilon_{\mathrm{M}}} f_0^{(s)}\right)^{-1} C^{(s)}[f^{(s)}, f^{(-s)}], \qquad [20]$$

where $f^{(s)} = f_0^{(s)} + \partial_{\epsilon_{\mathrm{M}}} f_0^{(s)} \cdot \eta^{(s)}$. At first, we neglect possible interactions between the nodes and consider properties of the collision operator acting on a well-defined chiral state $\hat{C}^{(s)}[\eta^{(s)}] \equiv \hat{C}^{(s)}[\eta^{(s)}, 0]$. This collision operator can be shown to be Hermitian and nonpositive with respect to the inner product (73, 90, 91)

$$\langle\eta|\zeta\rangle^{(s)} = -\int \frac{d^3p}{(2\pi\hbar)^3} D^{(s)}(\mathbf{p})\left(\partial_{\epsilon_{\mathrm{M}}} f_0^{(s)}\right)\eta(\mathbf{p})^*\zeta(\mathbf{p}). \qquad [21]$$

In the absence of an external magnetic field, $\mathbf{B} = 0$, the Fermi surface is a sphere and $D^{(s)}(\mathbf{p}) = 1$. Then, if we assume that the scattering in the bulk is isotropic, the problem is spherically symmetric and the eigenfunctions of $\hat{C}^{(s)}$ are the spherical harmonics

$$\hat{C}^{(s)}[Y_l^m(\hat{\mathbf{p}})] = -\Gamma_{l,m} Y_l^m(\hat{\mathbf{p}}) \quad (\mathbf{B} = 0). \qquad [22]$$

The eigenvalues $\Gamma_{l,m}$ describe the relaxation of the different modes. For example, if the distribution function $\eta^{(s)}$ is expanded in spherical harmonics as

$$\eta^{(s)} = \sum_{l,m} X_l^{m(s)} Y_l^m(\hat{\mathbf{p}}), \qquad [23]$$

where $X_l^{m(s)} = X_l^{m(s)}(\mathbf{x}, t)$ are some functions of position and time, the rate of change of the charge density is

$$\begin{aligned}\frac{d\rho^{(s)}}{dt} &= e\int \frac{d^3p}{(2\pi\hbar)^3}\frac{df^{(s)}(\mathbf{x},\mathbf{p},t)}{dt} \\ &= e\int \frac{d^3p}{(2\pi\hbar)^3}\partial_{\epsilon_{\mathrm{M}}} f_0^{(s)} \cdot \hat{C}^{(s)}[\eta^{(s)}] \\ &= -\frac{e\epsilon_{\mathrm{F}}^2}{(2\pi)^2\sqrt{\pi}\hbar^3 v^3}\Gamma_{0,0}\left(-X_0^{0(s)}\right).\end{aligned} \qquad [24]$$

A simple calculation shows that $\rho^{(s)} \propto -X_0^{0(s)}$. Thus, $\Gamma_{0,0}$ describes the rate of the particle number relaxation. Similarly, using the fact that $\hat{p}_z \propto Y_1^0(\hat{\mathbf{p}})$, $\hat{p}_x \propto \left(Y_1^{-1}(\hat{\mathbf{p}}) - Y_1^1(\hat{\mathbf{p}})\right)$, and $\hat{p}_y \propto i\left(Y_1^{-1}(\hat{\mathbf{p}}) + Y_1^1(\hat{\mathbf{p}})\right)$, it is easy to see that $\Gamma_{1,M}$, where $M = -1, 0, 1$ describe the rates of relaxation of momentum.

In the case of nonzero magnetic field, we can no longer use the spherical symmetry to find the eigenfunctions of the collision operator. Nevertheless, we can assume that they should be of the form $K_l^{m(s)} = Y_l^m + O(\alpha)$ and that the corresponding eigenvalues, $\Gamma_{0,0}$ and $\Gamma_{1,M}$, should again describe the rates of change of ρ and $\langle\mathbf{p}\rangle$, respectively. The details of finding the functions $K_l^{m(s)}$ can be found in *SI Appendix*. In this work we expand $K_l^{m(s)}$ in spherical harmonics to the second order in α.

Last, let us construct a collision operator that includes the relevant relaxation processes. One of them is the internode scattering, which transfers particles between the two nodes, leading to a dissipation of the axial charge; we denote the frequency at which this process happens by Γ_{inter}. Another process is the intranode scattering that, together with the internode scattering, relaxes momentum; we denote the total rate at which momentum is dissipated by Γ_{mr} and, consequently, we take $\Gamma_{1,M} = \Gamma_{\mathrm{mr}}$ for

$M=-1,0,+1$. Finally, we include in our analysis electron–electron scattering, which conserves momentum. Because modes with a high angular momentum do not contribute to the current, and to simplify the calculations, we assume a constant relaxation rate Γ_{tot} for all modes with the total angular momentum $L \geq 2$. All the scattering mechanisms that we consider, i.e., the inter- and intranode scattering, as well as the electron–electron collisions, contribute to Γ_{tot}. On the basis of the physical origin of the relaxation rates we take $\Gamma_{\text{inter}} < \Gamma_{\text{mr}} < \Gamma_{\text{tot}}$. Introducing the operators

$$\begin{aligned} P_0^{(s)} &= |K_0^{0(s)}\rangle\langle K_0^{0(s)}| - |K_0^{0(s)}\rangle\langle K_0^{0(-s)}|, \\ P_1^{(s)} &= \sum_{M=-1,0,1} |K_1^{M(s)}\rangle\langle K_1^{M(s)}|, \\ P_{\text{higher}}^{(s)} &= 1 - |K_0^{0(s)}\rangle\langle K_0^{0(s)}| - P_1^{(s)}, \end{aligned} \quad [25]$$

where s defines the distribution function that the operator acts on, the collision operator can be written as

$$\hat{C}^{(s)} = -\Gamma_{\text{inter}} P_0^{(s)} - \Gamma_{\text{mr}} P_1^{(s)} - \Gamma_{\text{tot}} P_{\text{higher}}^{(s)}. \quad [26]$$

Similar expansions of the collision operator were used in refs. 74–77 for different systems. It can be verified that with this choice of collision operator $\frac{d}{dt}\rho^{(s)} \propto -\Gamma_{\text{inter}}\left(\rho^{(s)} - \rho^{(-s)}\right)$ and, in the absence of external force and internode scattering, $\frac{d}{dt}\langle \mathbf{p}\rangle^{(s)} \propto -\Gamma_{\text{mr}}\langle \mathbf{p}\rangle^{(s)}$.

We are now in a position to write down the linearized Boltzmann equation (Eq. **10**). Recalling that we need to compute $\eta^{(s)}$ up to linear order in $\mathbf{E}$ and quadratic in $\mathbf{B}$, we can neglect the anomalous Hall term in the spatial-derivative term

$$\begin{aligned} &D^{(s)}(\hat{\mathbf{p}})\dot{\mathbf{x}}^{(s)} \cdot \partial_{\mathbf{x}} f^{(s)} \\ &\quad = \partial_{\epsilon_{\text{M}}} f_0^{(s)} \left[\mathbf{v}_{\text{M}}^{(s)} + e\hbar\left(\mathbf{v}_{\text{M}}^{(s)} \cdot \mathbf{\Omega}^{(s)}\right)\mathbf{B}\right] \cdot \partial_{\mathbf{x}} \eta^{(s)}, \end{aligned} \quad [27]$$

while the relevant contributions of the momentum-derivative term are

$$\begin{aligned} &D^{(s)}(\hat{\mathbf{p}})\dot{\mathbf{p}}^{(s)} \cdot \partial_{\mathbf{p}} f^{(s)} \\ &\quad = \left[e\mathbf{E} + e^2\hbar(\mathbf{E}\cdot\mathbf{B})\mathbf{\Omega}^{(s)}\right] \cdot \mathbf{v}_{\text{M}}^{(s)} \partial_{\epsilon_{\text{M}}} f_0 \\ &\quad + e\left[\mathbf{v}_{\text{M}}^{(s)} \times \mathbf{B}\right] \cdot \partial_{\mathbf{p}} \eta^{(s)} \partial_{\epsilon_{\text{M}}} f_0^{(s)}. \end{aligned} \quad [28]$$

Note that we use the formulas for $\mathbf{\Omega}^{(s)}$ and $\mathbf{v}_{\text{M}}^{(s)}$ given in Eqs. **18** and **19**, respectively, to account for the second-order corrections to the equations of motion. The last term on the RHS of Eq. **28** results from the Lorentz force and is the source of the classical Hall effect and classical magnetoresistance. Because these phenomena are well known and this article focuses on quantum corrections to the longitudinal conductivity, we do not include them here. Additionally, we are going to consider a setup where the electric field is parallel to the (external) magnetic field, in which case the classical magnetoresistance vanishes in the normal regime. On the other hand, in the hydrodynamic and ballistic regimes the situation is more complicated: For details, see *SI Appendix*. These considerations allow us to write the linearized Boltzmann equation

$$\begin{aligned} &D^{(s)}\partial_t \eta^{(s)} + \left[\mathbf{v}_{\text{M}}^{(s)} + e\hbar\left(\mathbf{v}_{\text{M}}^{(s)} \cdot \mathbf{\Omega}^{(s)}\right)\mathbf{B}\right] \cdot \partial_{\mathbf{x}} \eta^{(s)} \\ &\quad + e\left[\mathbf{E}\cdot\mathbf{v}_{\text{M}}^{(s)} + e\hbar(\mathbf{E}\cdot\mathbf{B})\left(\mathbf{\Omega}^{(s)} \cdot \mathbf{v}_{\text{M}}^{(s)}\right)\right] \\ &\quad = D^{(s)}\hat{C}^{(s)}[\eta^{(s)}, \eta^{(-s)}], \end{aligned} \quad [29]$$

with $\hat{C}^{(s)}$ defined in Eq. **26**.

Bulk Conductivities

In this section, we calculate the current flowing through the bulk of a Weyl semimetal subject to a weak ac electric field. The material is modeled as an infinite half-space $z > 0$, while $z < 0$ is the vacuum. We place the material in a static external magnetic field parallel to the surface, $\mathbf{B} = B\hat{\mathbf{x}}$, and consider an oscillating electric field propagating through the bulk and polarized in the same direction as the magnetic field: $\mathbf{E}(z,t) = E(z,t)\hat{\mathbf{x}}$. The electric field is assumed to be uniform in the *xy* plane.

The general expression for the current, after taking into account the orbital magnetization, can be written as

$$\mathbf{J} = \mathbf{J}_{\text{kin}} + \mathbf{J}_{\text{magn}}, \quad [30]$$

where $\mathbf{J}_{\text{kin}}$ is given by Eq. **9** and represents the "kinematic" part resulting from the forward motion of the wavepackets, while

$$\mathbf{J}_{\text{magn}} = \nabla \times \sum_{s=\pm 1} \int \frac{d^3p}{(2\pi)^3} D^{(s)}(\mathbf{p}) \frac{se\hbar v}{2|\mathbf{p}|} \hat{\mathbf{p}} f^{(s)}(q,\mathbf{p}) \quad [31]$$

is the magnetization current. However, in the setup that we consider $\mathbf{J}_{\text{magn}} = 0$ (see *SI Appendix* for a proof). Consequently, in what follows

$$\mathbf{J} = \mathbf{J}_{\text{kin}}. \quad [32]$$

Eq. **9** is now expanded to the second order in α. In this article we neglect the anomalous Hall effect, i.e., the $e\hbar\mathbf{E} \times \mathbf{\Omega}^{(s)}$ term. In a time-reversal symmetry-breaking Weyl semimetal with a single pair of nodes this can be justified, if the electric field is aligned parallel (or near parallel) to the vector connecting the Weyl nodes in reciprocal space. After switching to spherical coordinates (p,θ,ϕ) in momentum space, one obtains

$$\begin{aligned} \mathbf{J}(z) &= e\sum_{s=\pm 1} \int \frac{d^3p}{(2\pi\hbar)^3} D(\mathbf{p})\dot{\mathbf{x}}(\mathbf{p})(-\delta\left[\epsilon_{\text{M}}(\mathbf{p}) - \epsilon_{\text{F}}\right])\eta(z,\mathbf{p}) \\ &= -\frac{e\epsilon_{\text{F}}^2}{v^2(2\pi\hbar)^3} \sum_{s=\pm 1} \int d(\cos\theta)\, d\phi \\ &\quad \left[\hat{\mathbf{p}} + 3s\alpha(\hat{\mathbf{p}}\cdot\hat{\mathbf{b}})\hat{\mathbf{p}} - \alpha^2\hat{\mathbf{p}} + \alpha^2(\hat{\mathbf{p}}\cdot\hat{\mathbf{b}})\hat{\mathbf{b}}\right]\eta^{(s)}(z,\hat{\mathbf{p}}), \end{aligned} \quad [33]$$

where we suppress the (s) labels on all quantities in the first line.

To find the current from Eq. **33**, the distribution functions $\eta^{(s)}(z,\mathbf{p})$ have to be determined from the Boltzmann equation (Eq. **29**). We shall work with Fourier-transformed quantities defined as follows:

$$\begin{aligned} \eta^{(s)}(z,\mathbf{p},t) &= \int d\omega\, dq e^{i\omega t - iqz}\eta^{(s)}(q,\mathbf{p},\omega), \\ \mathbf{E}(z,\mathbf{p},t) &= \int d\omega\, dk e^{i\omega t - iqz}\mathbf{E}(q,\mathbf{p},\omega). \end{aligned} \quad [34]$$

The Boltzmann equation is solved perturbatively in α after expanding the out-of-equilibrium distribution in spherical harmonics as

$$\eta^{(s)} = \sum_{l,m}\left(A_l^m + s\alpha B_l^m + \alpha^2 C_l^m\right) Y_l^m(\hat{\mathbf{p}}). \quad [35]$$

Next, the collision integral on the RHS of Eq. **29** is evaluated using the definition of the inner product 21; the expansion of the collision operator into projection operators 25, 26; and the form of the eigenvectors $K_l^{m(s)}$ determined in *SI Appendix*. Then, Eq. **29** is projected onto a spherical harmonic of degree L and

order M by multiplying both sides by $Y_L^{M*}(\hat{\mathbf{p}})$ and integrating over the angles. These integrals can be evaluated analytically, producing an infinite system of equations labeled by L, M. Finally, terms that are of the same order in α are equated, leading to three systems of equations (for terms of order 1, α, and α^2) that are solved in turn.

We now solve the system of equations corresponding to the lowest level of approximation ($\alpha = 0$) to demonstrate the general strategy of solution, which is in the same spirit as the one used in ref. 92 for a two-dimensional (2D) system. At this level, the equations are*

$$i\omega A_0^0 - iqv\frac{\sqrt{3}}{3}A_1^0 = 0, \qquad [36]$$

$$(i\omega + \Gamma_{\text{mr}})\, A_1^0 - iqv\left[\frac{\sqrt{3}}{3}A_0^0 + \sqrt{\frac{4}{15}}A_2^0\right] = 0, \qquad [37]$$

$$(i\omega + \Gamma_{\text{mr}})A_1^{\pm 1} - iqv\frac{\sqrt{5}}{5}A_2^{\pm 1} \mp ev\sqrt{\frac{2\pi}{3}}E = 0, \qquad [38]$$

$$(i\omega + \Gamma_{\text{tot}})\, A_L^M - iqv\frac{1}{2}\left[A_{L-1}^M + A_{L+1}^M\right] = 0 \quad (\text{for } L \geq 2). \qquad [39]$$

Note that in the above, due to the cylindrical symmetry of the system in the absence of an electric field, only equations for a fixed M are coupled. Eq. **39** is a recurrence relation that can be solved by the ansatz $A_L^M = r^{L-1}A_1^M$. There are two solutions, from which we choose the one that ensures convergence of the series,

$$r = -\frac{i}{qv}\left[\Gamma_{\text{tot}} + i\omega - \sqrt{(\Gamma_{\text{tot}} + i\omega)^2 + q^2v^2}\right], \qquad [40]$$

where we take the square root in the bracket to return a value with a positive real and a positive imaginary part. Inserting $A_2^M = rA_1^M$ for $M = -1, 0, +1$ in Eqs. **36–38** yields a closed system of equations that can easily be solved, while for $|M| > 1$ the solution is trivial: $A_L^M = 0$. This way, the full distribution function at the classical level is found to be

$$A_1^{\pm 1} = \pm\sqrt{\frac{2\pi}{3}}\frac{evE}{\Gamma_{\text{mr}} + i\omega - \frac{\sqrt{5}}{5}iqvr}, \qquad [41]$$
$$A_L^{\pm 1} = r^{L-1}A_1^{\pm 1}, \qquad A_L^{M\neq\pm 1} = 0.$$

The same procedure can be used to find corrections to $\eta^{(s)}$ at higher orders in α as well. First, the solution for A_L^M is plugged into the equations that are linear in α to find B_L^M. Subsequently, the equations for high L are expressed as a recurrence relation that is then solved, and its solution is used to turn the system of equations for $L = 0, 1, 2$ into a closed system. After solving this system, the solutions for A_L^M and B_L^M are plugged into the quadratic-order equations to find C_L^M and the procedure is repeated. As the calculations are lengthy and not particularly instructive, we relegate the details to *SI Appendix*.

After finding the distributions $\eta^{(s)}(q, \hat{\mathbf{p}}, \omega)$, the current is evaluated using Eq. **33**. The current can be expressed as $\mathbf{J}(q, \omega) = \sigma(q, \omega)\mathbf{E}(q, \omega)$, where the conductivity σ is a complicated function of q and ω. Here we present only the formulas for the conductivity in the limiting cases, in which some of the frequency scales involved in the problem are much greater than the others. The relevant frequency scales are the relaxation rates, which satisfy the inequalities $\Gamma_{\text{inter}} < \Gamma_{\text{mr}} < \Gamma_{\text{tot}}$, ω (the driving frequency), and qv. As both qv and ω can in general be placed between any two relaxation rates in this chain of inequalities, there are in principle a large number of limiting cases that can be considered. Instead of analyzing each one of them, we focus only on the regimes that could be accessed in a skin effect experiment, which we identify in the following way. We choose certain realistic material parameters, close to those reported for WP_2 (40, 93): $v = 1.4 \times 10^5$ m/s, $\epsilon_{\text{F}} = 20$ meV, $\Gamma_{\text{mr}} = 10^9$ Hz, $\Gamma_{\text{tot}} = 10^{10}$ Hz. We moreover assume that Γ_{inter} is two orders of magnitude smaller than Γ_{mr} as reported for TaAs (26), so $\Gamma_{\text{inter}} = 10^7$ Hz. Next, let us note that the classical conductivity can be calculated using Eqs. **41** and **33** evaluated at the classical (i.e., $\alpha = 0$) level, yielding

$$\sigma_{\text{cl}}(q, \omega) = 2\,\varepsilon\,\omega_{\text{P}}^2\frac{1}{\Gamma_{\text{mr}} + i\omega - \frac{\sqrt{5}}{5}iqvr}, \qquad [42]$$

where the plasma frequency ω_{P} is defined by

$$\omega_{\text{P}}^2 = \frac{e^2\epsilon_{\text{F}}^2}{6\pi^2\varepsilon\hbar^3 v} \qquad [43]$$

and ε is the electric permittivity of the medium. Then, we can solve the Fourier-transformed Eq. **2** as

$$\left(-q^2 + \frac{\omega^2}{c^2}\right) = i\,\mu\,\omega\,\sigma(q, \omega)_{\text{cl}} \qquad [44]$$

to obtain the wavectors q, which correspond to modes that can propagate through the bulk, as a function of ω. This equation has in general six solutions, but we can restrict our attention to those with a negative imaginary part and a positive real part, which in accordance with Eq. **34** correspond to modes propagating in the positive direction along z and decaying with the distance. It turns out that out of the six solutions one satisfies this condition for all ω, and one satisfies it at high frequencies only; we denote these solutions q_1 and q_2, respectively. The characteristic length scales at which these modes decay, defined as $\delta_i = -\text{Im}[q_i]^{-1}$, can be used as a proxy for the classical skin depth and they are plotted in Fig. 2. Based on the different scaling of q_i with ω we can identify four relevant regimes, which we call low-frequency normal, hydrodynamic, ballistic, and high-frequency normal. In all these regimes, except the last one, ω is smaller than all the relevant frequency scales and can thus be neglected in the analysis.

When quantum effects are included, the low-frequency normal regime splits into two, as discussed in the Introduction. The different regimes and the corresponding conductivities are assembled in Table 1. It can be seen that while in both the low-frequency normal and the anomaly-induced nonlocal regimes the relaxation of momentum and axial charge are related to different frequency scales, in the other regimes they both happen at a comparable rate.

We can extract further information as to the origin of the numerical coefficients in Table 1 if before the start of the calculations we multiply the term corresponding to the OMM in Eq. **11** (that is, $-s\frac{e\hbar\mathbf{B}\cdot\mathbf{p}}{2|\mathbf{p}|^2}$) by a factor ξ_1, and similarly we multiply all the terms resulting from the second-order corrections to the energy and Berry curvature in Eqs. **11** and **12** by ξ_2, and then we keep track of these coefficients during the computations. This allows us to determine the following:

- The second-order corrections to the equations of motion have no influence on the conductivity either in the normal or the AIN regimes, affecting only the hydrodynamic and ballistic results.

*The factor of 1/2 in front of the bracket in the last equation is in fact an approximate value, but this approximation works very well here. For a discussion of this approximation, see *SI Appendix*.

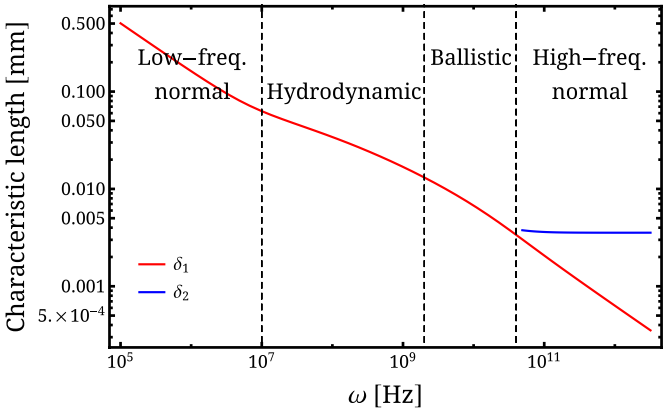

Fig. 2. Dependence of the characteristic length scales at which a propagating electric field decays on ω. The two curves represent two solutions of Maxwell's equations in the form of Eq. **44** supplemented by the formula for the classical conductivity Eq. **42** and experimentally realistic parameters (main text): $v = 1.4 \times 10^5$ m/s, $\epsilon_F = 20$ meV, $\Gamma_{mr} = 10^9$ Hz, and $\Gamma_{tot} = 10^{10}$ Hz. We select only solutions satisfying $\mathrm{Re}[q_i] > 0$, $\mathrm{Im}[q_i] < 0$ and plot their characteristic decay lengths, defined as $\delta_i = -\mathrm{Im}[q_i]^{-1}$. At low frequencies there exists only one solution q_1 satisfying these conditions. We can observe three transport regimes (identified as low-frequency normal, hydrodynamic, and ballistic) where δ_1 shows different scaling with ω, and the cross-overs (marked with dashed black lines) happen around the values of ω for which $|q_1 v| \approx \Gamma_{mr}$ and $|q_1 v| \approx \Gamma_{tot}$. Above a certain value of ω, around the point when $|q_1 v| \approx \omega$, another solution q_2 becomes relevant. Since δ_2 is the longer of the two decay lengths, it dominates the propagation of the electric field and we are in what we call the high-frequency normal regime.

- For a relatively high Γ_{inter}, namely $\Gamma_{inter} > 15\Gamma_{mr}/22 \approx 0.7\Gamma_{mr}$, the magnetoconductivity in the low-frequency regime changes sign from positive to negative, in qualitative agreement with refs. 83 and 84. This is found to be caused by the contribution of the OMM, as setting $\xi_1 = 0$ and neglecting electron–electron collisions (so that $\Gamma_{tot} = \Gamma_{mr}$) would result in a different formula for the conductivity, denoted here as $\tilde{\sigma}$,

$$\tilde{\sigma}(q,\omega) = \varepsilon\,\omega_P^2 \left[\frac{2}{\Gamma_{mr}} + \alpha^2 \frac{3}{\Gamma_{inter}} - \alpha^2 \frac{42}{15}\frac{1}{\Gamma_{mr}}\right], \qquad [45]$$

  and the magnetoconductivity would always be positive, again in agreement with refs. 83 and 84.
- In the hydrodynamic regime the large negative coefficient is also due to the OMM as setting $\xi_1 = 0$ would result in a positive coefficient

$$\tilde{\sigma}(q,\omega) \approx \varepsilon\,\omega_P^2 \frac{\Gamma_{tot}}{q^2 v^2}\left[9.0 + 5.2\alpha^2\right]. \qquad [46]$$

- In contrast, magnetoconductivity in the AIN regime is not affected by either the OMM or the second-order corrections and results solely from the leading-order term in the Berry curvature. The nonlocality of the quantum correction to the conductivity can be seen in its dependence on q, absent in the classical part.

Skin Effect

To find the skin depths and the surface impedance in the regimes identified in the previous section, we have to include the presence of a boundary in our analysis. This is done by imposing appropriate boundary conditions on the distribution functions. As a particularly simple choice we impose specular boundary conditions, meaning that during reflection the transverse components of velocity stay the same but the perpendicular component gets inverted; i.e., $\eta^{(s)}(z=0, v_x, v_y, v_z) = \eta^{(s)}(z=0, v_x, v_y, -v_z)$. These boundary conditions can be naturally implemented if, following ref. 42, we add a mirror-symmetric counterpart (for $z < 0$) to the original (physical) half-space system. Then, in the augmented setup the condition of specular reflection means that the particles move freely across the $z = 0$ boundary (Fig. 3). Because the electric field is parallel to the surface, its mirror-reflected components are related by $\mathbf{E}(-z,t) = \mathbf{E}(z,t)$. Furthermore, the external magnetic field $\mathbf{B}$ does not change under the mirror reflection, which allows us to use a single formula for the conductivity in the whole space.

From Maxwell's equations we obtain the relation (using $\mathbf{E}(z,t) = E(z,t)\hat{\mathbf{x}}$)

$$\partial_z^2 E(z,t) = \frac{1}{c^2}\partial_t^2 E(z,t) + \mu\partial_t J(z,t). \qquad [47]$$

Fourier transforming the left-hand side (LHS),

$$\int_{-\infty}^{\infty} \frac{dz}{2\pi} E''(z) e^{iqz} = \int_{-\infty}^{\infty} \frac{dz}{2\pi}\left(E'(z)e^{iqz}\right)' dz - iq\int_{-\infty}^{\infty}\frac{dz}{2\pi}E'(z)e^{iqz}\,dz. \qquad [48]$$

The first derivative of $E(z)$ has a discontinuity at $z = 0$, so that $E'(z=0^-) = -E'(z=0^+)$, which means that the integration of the first term should be done separately in $(-\infty, 0)$ and $(0, \infty)$. The second term can be integrated by parts once again, producing

$$\int_{-\infty}^{\infty} \frac{dz}{2\pi} E''(z) e^{iqz} = -\frac{1}{\pi}E'(z=+0) - q^2 E(q). \qquad [49]$$

Table 1. Conductivity and surface impedance in the different regimes and their regions of validity

Regime	Valid when	Conductivity $\sigma(q,\omega)$	Surface impedance $Z(\omega)$
Low-frequency			
normal	$q^2v^2 \ll \Gamma_{inter}\Gamma_{mr}\ \omega \ll \Gamma_{inter}$	$\varepsilon\,\omega_P^2\left[\frac{2}{\Gamma_{mr}} + \alpha^2\frac{3}{\Gamma_{inter}} - \alpha^2\frac{66}{15}\frac{1}{\Gamma_{mr}}\right]$	$e^{i\pi/4}\mu\sqrt{\frac{\omega c^2}{\omega_P^2}}\left(\frac{2}{\Gamma_{mr}} + \alpha^2\frac{3}{\Gamma_{inter}} - \alpha^2\frac{66}{15}\frac{1}{\Gamma_{mr}}\right)^{-\frac{1}{2}}$
Anomaly-induced			
nonlocal	$\Gamma_{inter}\Gamma_{mr} \ll q^2v^2 \ll \Gamma_{mr}^2\ \omega \ll q^2v^2/\Gamma_{mr}$	$\varepsilon\,\omega_P^2\left[\frac{2}{\Gamma_{mr}} + \alpha^2\frac{18\Gamma_{mr}}{q^2v^2}\right]$	See Eq. **56**
Hydrodynamic	$\Gamma_{mr}\Gamma_{tot} \ll q^2v^2 \ll \Gamma_{tot}^2\ \omega \ll q^2v^2/\Gamma_{tot}$	$\varepsilon\,\omega_P^2\frac{\Gamma_{tot}}{q^2v^2}\left[9.0 - 26\alpha^2\right]$	$\frac{1}{2}\left(e^{i\pi/8} + e^{i5\pi/8}\right)\mu\left(\frac{\omega^3v^2c^2}{\omega_P^2\Gamma_{tot}\left[9.0-26\alpha^2\right]}\right)^{1/4}$
Ballistic	$\Gamma_{tot} \ll qv\ \omega \ll qv$	$\varepsilon\,\omega_P^2\frac{1}{qv}\left[4.5 + 4.3\alpha^2\right]$	$\frac{4\sqrt{3}}{9}e^{i\pi/3}\mu\left(\frac{\omega^2vc^2}{\omega_P^2\left[4.5+4.3\alpha^2\right]}\right)^{1/3}$
High-frequency			
normal	$qv \ll \omega\ \Gamma_{tot} \ll \omega$	$-i\varepsilon\,\omega_P^2\frac{1}{\omega}\left[2 + \frac{8}{5}\alpha^2\right]$	$-i\mu\frac{\omega c}{\omega_P}\left(2 + \frac{8}{5}\alpha^2\right)^{-\frac{1}{2}}$

The numerical coefficients in the hydrodynamic and ballistic regimes are rounded up to two significant numbers.

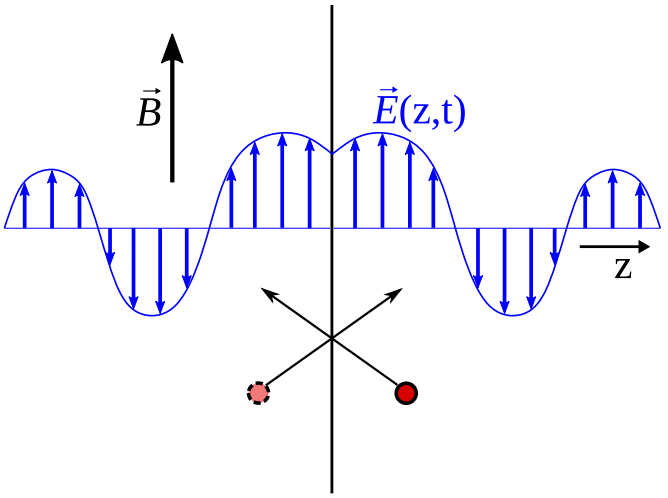

Fig. 3. Implementation of specular boundary conditions. To the original system located in $z > 0$ its mirror-reflected version is added in $z < 0$, which creates a discontinuity in the derivative of the electric field at the boundary. A specular reflection of a particle can be seen as its mirror-reflected counterpart freely crossing the boundary.

The Fourier transform of $J(z,\omega)$ is $\sigma(q,\omega)E(q,\omega)$, where $\sigma(q,\omega)$ was determined in the previous section, so from Eq. **47** we obtain

$$E(q,\omega) = \frac{-E'(z=0^+)}{\pi} \frac{1}{q^2 - \frac{\omega^2}{c^2} + i\mu\omega\sigma(|q|,\omega)}, \quad \textbf{[50]}$$

where we explicitly write $|q|$ because conductivity has to be an even function of q. Finally, we obtain

$$\begin{aligned} E(z) &= -\frac{E'(z=0^+)}{\pi} \int_{-\infty}^{\infty} dq \frac{e^{-iqz}}{q^2 - \frac{\omega^2}{c^2} + i\mu\omega\sigma(|q|,\omega)} \\ &= -\frac{2E'(z=0^+)}{\pi} \int_{0}^{\infty} dq \frac{e^{-iqz}}{q^2 - \frac{\omega^2}{c^2} + i\mu\omega\sigma(q,\omega)}. \end{aligned} \quad \textbf{[51]}$$

This result allows us to calculate surface impedance, defined as (94)

$$Z = \frac{E(z=0)}{\int_0^\infty J(z)dz}. \quad \textbf{[52]}$$

Using Maxwell's equations this formula can be rewritten as

$$Z = -i\mu\omega \frac{E(z=0)}{E'(z=0^+)}. \quad \textbf{[53]}$$

As the conductivities in all the regimes except AIN show only quantitative changes with respect to their classical counterparts, we restrict ourselves to presenting the impedances obtained from Eqs. **53** and **51** in Table 1.

Skin Effect in the AIN Regime. We now present a detailed analysis of the skin effect in the most interesting case of the anomaly-induced nonlocal regime. In fact, we can also capture the crossover from the low-frequency normal regime by approximating the conductivity as

$$\sigma(q,\omega) \approx \sigma_0 \left[1 + \alpha^2 \frac{\Gamma_{\rm mr}}{2\Gamma_{\rm inter}/3 + q^2v^2/9\Gamma_{\rm mr}}\right], \quad \textbf{[54]}$$

where $\sigma_0 = 2\epsilon\omega_{\rm p}^2/\Gamma_{\rm mr}$. This approximation for the conductivity works only when $\Gamma_{\rm inter} \ll \Gamma_{\rm mr}$, $qv \ll \Gamma_{\rm mr}$, and $\omega \ll q^2v^2/\Gamma_{\rm mr}$.

We want to evaluate the integral in Eq. **51**, which can be done using standard contour integration methods. The resulting impedance in both the low-frequency normal and the AIN regimes can be seen in Fig. 4.

The AIN regime can be observed when $(\omega\mu\sigma_0)v^2 \gg \Gamma_{\rm mr}\Gamma_{\rm inter}$. For $z = 0$ we integrate over the contour in the lower half-plane, and thus we are interested in the poles with a negative imaginary part. There are two such poles: $q_1 \approx e^{-i\pi/4}\sqrt{\mu\omega\sigma_0 + i\alpha^2\frac{9\Gamma_{\rm mr}^2}{v^2}}$ and $q_2 \approx -i\sqrt{\Gamma_{\rm mr}(6\Gamma_{\rm inter} + 9\alpha^2\Gamma_{\rm mr})}/v$. Please note that $|q_2| \ll |q_1|$. The electric field is

$$E(z) = iE'(z=0^+)\left[\frac{\exp(-iq_1z)}{q_1} + \alpha^2\frac{9\Gamma_{\rm mr}^2}{q_1^2v^2}\frac{\exp(-iq_2z)}{q_2}\right]. \quad \textbf{[55]}$$

This result shows that there is an anomalous component of the electric field with the skin depth much larger than the classical skin depth, so at large distances the anomalous component dominates over the classical one. The impedance is then

$$Z = e^{i\pi/4}\sqrt{\frac{\mu\omega}{\sigma_0 + i\alpha^2\frac{9\Gamma_{\rm mr}^2}{\mu\omega v^2}}} - \alpha^2\frac{9\Gamma_{\rm mr}}{\sigma_0 v}\left(6\frac{\Gamma_{\rm inter}}{\Gamma_{\rm mr}} + 9\alpha^2\right)^{-\frac{1}{2}}. \quad \textbf{[56]}$$

Therefore, in a finite magnetic field the impedance in this regime no longer scales with the square root of ω, as seen in Fig. 4. This regime with its characteristic impedance is a central finding of the present article.

Discussion and Conclusions

We provided a detailed analysis of the chiral magnetic conductivity across various transport regimes. To do so, we constructed a collision operator that captures three different relaxation mechanisms by exploiting its algebraic properties. We also included in our analysis second-order semiclassical corrections. The computed conductivities show a quantitative influence of these corrections in the hydrodynamic and anomalous regimes, although it has to be

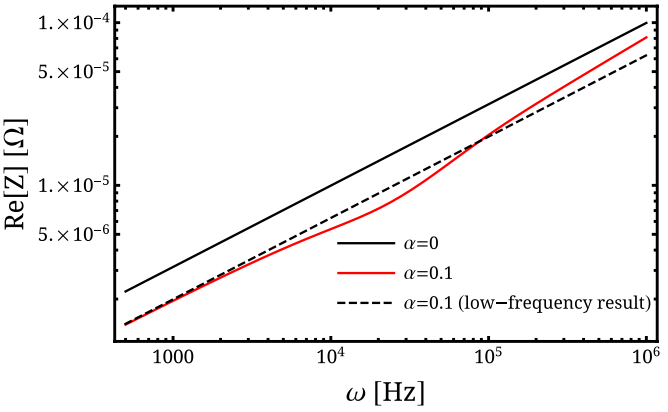

Fig. 4. Dependence of the real part of the surface impedance Z on frequency ω in the low-frequency normal and the AIN regimes, obtained from Eqs. **53**, **51**, and **54** in the cases of no magnetic field ($\alpha = 0$) and a nonzero magnetic field ($\alpha = 0.1$). The dashed line is plotted on the basis of the impedance of the low-frequency normal regime as found in Table 1, and it is the result that would be measured in the absence of the nonlocal behavior. The material parameters are $v = 1.4 \times 10^5$ m/s, $\epsilon_{\rm F} = 20$ meV, $\Gamma_{\rm mr} = 10^9$ Hz, and $\Gamma_{\rm inter} = 10^7$ Hz. The transition to the AIN regime takes place around $\omega = 10^5$ Hz. We see that changing the external magnetic field leads to a noticeable change of the surface impedance, especially shortly before the onset of the AIN regime, and moreover in this regime the scaling with frequency changes with respect to the no-field result.

noted that due to the coexistence of classical magnetoconductivity in these regimes, the quantum corrections could be difficult to separate out experimentally.

More importantly, we uncovered an entirely different transport regime where the conductivity is a combination of a classical local part and a nonlocal quantum part. This leads to a change of scaling of the surface impedance with the driving frequency when the material is placed in an external magnetic field. This phenomenon is related to a significant increase in the skin depth, which might be possible to observe in thin enough samples.

In the end, we note that there are various other phenomena that affect transport in Weyl semimetals that we did not include in our analysis. We neglected the influence of the Fermi arcs and the anomalous Hall effect (which plays a significant role in the propagation of light in time-reversal symmetry-breaking Weyl semimetals), as well as all the effects nonlinear in the electric field. Nonetheless, the results of this article hold for time-reversal symmetry-breaking Weyl semimetals placed in weak fields when the positions of the nodes are properly aligned with the electric field, as well as (qualitatively) for noncentrosymmetric Weyl semimetals. In particular, the presence of the anomaly-induced nonlocal regime should be discernible experimentally.

Our work serves as a starting point for detailed analyses of transport regimes in Weyl semimetals, including different scattering mechanisms relevant for realistic experimental situations. As a result, one can construct a detailed theoretical description of a generation of transport measurements beyond two-dimensional analogs. This allows one to investigate effects absent in two dimensions, such as chiral vortical effect or anomalous thermal transport. It also permits one to include realistic boundary conditions, important in electron hydrodynamics and usually neglected in high-energy applications of chiral kinetic theory.

Note. When this article was being prepared, a preprint appeared (95), in which the existence of a nonlocal regime with the same qualitative features as the AIN regime was predicted. While ref. 95, contrary to the present work, assumes $\omega \gg \Gamma_{\text{inter}}$, it is worth noting that when Γ_{inter} is replaced with $i\omega/2$ in Eq. **55**, the results of the two articles are found to be in good agreement.

Data Availability. There are no data underlying this work.

ACKNOWLEDGMENTS. We acknowledge discussions with Francisco Peña-Benitez, Peng Rao, and Jörg Schmalian. We thank Pavlo Sukhachov for comments on the manuscript. This work was in part supported by the Deutsche Forschungsgemeinschaft through the Leibniz Program, the cluster of excellence ct.qmat (Exzellenzcluster [EXC] 2147, Project 39085490), and Sonderforschungsbereich (SFB) 1143 (Project 247310070). P.S. was also supported by the Narodowe Centrum Nauki Sonata Bis Grant 2019/34/E/ST3/00405.

Author affiliations: [a]Max Planck Institute for the Physics of Complex Systems, 01187 Dresden, Germany; [b]Würzburg-Dresden Cluster of Excellence Complexity and Topology in Quantum Matter (ct.qmat), 01187 Dresden, Germany; [c]Department of Physics, University of Basel, 4056 Basel, Switzerland; and [d]Department of Theoretical Physics, Wrocław University of Science and Technology, 50-370 Wrocław, Poland

1. R. N. Gurzhi, Minimum of resistance in impurity-free conductors. *Sov. Phys. JETP* **44**, 771–772 (1963).
2. R. N. Gurzhi, Hydrodynamic effects in solids at low temperature. *Sov. Phys. Usp.* **11**, 255–270 (1968).
3. L. Molenkamp, M. de Jong, Observation of Knudsen and Gurzhi transport regimes in a two-dimensional wire. *Solid-State Electron.* **37**, 551–553 (1994).
4. M. J. de Jong, L. W. Molenkamp, Hydrodynamic electron flow in high-mobility wires. *Phys. Rev. B Condens. Matter* **51**, 13389–13402 (1995).
5. G. M. Gusev, A. D. Levin, E. V. Levinson, A. K. Bakarov, Viscous transport and Hall viscosity in a two-dimensional electron system. *Phys. Rev. B* **98**, 161303 (2018).
6. J. Crossno *et al.*, Observation of the Dirac fluid and the breakdown of the Wiedemann-Franz law in graphene. *Science* **351**, 1058–1061 (2016).
7. D. A. Bandurin *et al.*, Negative local resistance caused by viscous electron backflow in graphene. *Science* **351**, 1055–1058 (2016).
8. D. A. Bandurin *et al.*, Fluidity onset in graphene. *Nat. Commun.* **9**, 4533 (2018).
9. J. A. Sulpizio *et al.*, Visualizing Poiseuille flow of hydrodynamic electrons. *Nature* **576**, 75–79 (2019).
10. A. I. Berdyugin *et al.*, Measuring Hall viscosity of graphene's electron fluid. *Science* **364**, 162–165 (2019).
11. M. J. H. Ku *et al.*, Imaging viscous flow of the Dirac fluid in graphene. *Nature* **583**, 537–541 (2020).
12. A. C. Keser *et al.*, Geometric control of universal hydrodynamic flow in a two-dimensional electron fluid. *Phys. Rev. X* **11**, 031030 (2021).
13. B. N. Narozhny, I. V. Gornyi, A. D. Mirlin, J. Schmalian, Hydrodynamic approach to electronic transport in graphene. *Ann. Phys.* **529**, 1700043 (2017).
14. A. Lucas, K. C. Fong, Hydrodynamics of electrons in graphene. *J. Phys. Condens. Matter* **30**, 053001 (2018).
15. N. P. Armitage, E. J. Mele, A. Vishwanath, Weyl and Dirac semimetals in three-dimensional solids. *Rev. Mod. Phys.* **90**, 015001 (2018).
16. H. Nielsen, M. Ninomiya, Absence of neutrinos on a lattice: (i). Proof by homotopy theory. *Nucl. Phys. B* **185**, 20–40 (1981).
17. H. Nielsen, M. Ninomiya, The Adler-Bell-Jackiw anomaly and Weyl fermions in a crystal. *Phys. Lett. B* **130**, 389–396 (1983).
18. R. A. Bertlmann, *Anomalies in Quantum Field Theory* (International Series of Monographs on Physics, Oxford University Press, Oxford, UK, 2000).
19. K. Landsteiner, Notes on anomaly induced transport. *Acta Phys. Pol. B* **47**, 2617 (2016).
20. X. Huang *et al.*, Observation of the chiral-anomaly-induced negative magnetoresistance in 3D Weyl semimetal TaAs. *Phys. Rev. X* **5**, 031023 (2015).
21. C. Z. Li *et al.*, Giant negative magnetoresistance induced by the chiral anomaly in individual Cd3As2 nanowires. *Nat. Commun.* **6**, 10137 (2015).
22. H. Li *et al.*, Negative magnetoresistance in Dirac semimetal Cd3As2. *Nat. Commun.* **7**, 10301 (2016).
23. Q. Li *et al.*, Chiral magnetic effect in ZrTe5. *Nat. Phys.* **12**, 550–554 (2016).
24. H. J. Kim *et al.*, Dirac versus Weyl fermions in topological insulators: Adler-Bell-Jackiw anomaly in transport phenomena. *Phys. Rev. Lett.* **111**, 246603 (2013).
25. J. Xiong *et al.*, Evidence for the chiral anomaly in the Dirac semimetal Na_3Bi. *Science* **350**, 413–416 (2015).
26. C. L. Zhang *et al.*, Signatures of the Adler-Bell-Jackiw chiral anomaly in a Weyl fermion semimetal. *Nat. Commun.* **7**, 10735 (2016).
27. S. Liang *et al.*, Experimental tests of the chiral anomaly magnetoresistance in the Dirac-Weyl semimetals na3bi and GdPtBi. *Phys. Rev. X* **8**, 031002 (2018).
28. R. M. A. Dantas, F. Peña-Benitez, B. Roy, P. Surówka, Magnetotransport in multi-Weyl semimetals: A kinetic theory approach. *J. High Energy Phys.* **2018**, *69* (2018).
29. K. Fukushima, D. E. Kharzeev, H. J. Warringa, Chiral magnetic effect. *Phys. Rev. D* **78**, 074033 (2008).
30. D. E. Kharzeev, H. J. Warringa, Chiral magnetic conductivity. *Phys. Rev. D* **80**, 034028 (2009).
31. N. Banerjee *et al.*, Hydrodynamics from charged black branes. *J. High Energy Phys.* **2011**, 94 (2011).
32. J. Erdmenger, M. Haack, M. Kaminski, A. Yarom, Fluid dynamics of R-charged black holes. *J. High Energy Phys.* **2009**, 055 (2009).
33. Y. Neiman, Y. Oz, Relativistic hydrodynamics with general anomalous charges. *J. High Energy Phys.* **2011**, 23 (2011).
34. D. T. Son, P. Surówka, Hydrodynamics with triangle anomalies. *Phys. Rev. Lett.* **103**, 191601 (2009).
35. K. Landsteiner, E. Megías, F. Peña-Benitez, Gravitational anomaly and transport phenomena. *Phys. Rev. Lett.* **107**, 021601 (2011).
36. A. Lucas, R. A. Davison, S. Sachdev, Hydrodynamic theory of thermoelectric transport and negative magnetoresistance in Weyl semimetals. *Proc. Natl. Acad. Sci. U.S.A.* **113**, 9463–9468 (2016).
37. E. V. Gorbar, V. A. Miransky, I. A. Shovkovy, P. O. Sukhachov, Hydrodynamic electron flow in a Weyl semimetal slab: Role of Chern-Simons terms. *Phys. Rev. B* **97**, 205119 (2018).
38. R. M. A. Dantas, F. Peña-Benitez, B. Roy, P. Surówka, Non-abelian anomalies in multi-Weyl semimetals. *Phys. Rev. Res.* **2**, 013007 (2020).
39. N. P. Ong, S. Liang, Experimental signatures of the chiral anomaly in Dirac–Weyl semimetals. *Nat. Rev. Phys* **3**, 394–404 (2021).
40. J. Gooth *et al.*, Thermal and electrical signatures of a hydrodynamic electron fluid in tungsten diphosphide. *Nat. Commun.* **9**, 4093 (2018).
41. U. Vool *et al.*, Imaging phonon-mediated hydrodynamic flow in WTe2. *Nat. Phys.* **17**, 1216–1220 (2021).
42. E. M. Lifshitz, L. P. Pitaevskii, *Physical Kinetics* (Pergamon, 1981).
43. R. Soto, *Kinetic Theory and Transport Phenomena* (Oxford University Press, 2016).
44. R. Loganayagam, P. Surówka, Anomaly/transport in an Ideal Weyl gas. *J. High Energy Phys.* **2012**, 97 (2012).
45. D. T. Son, N. Yamamoto, Berry curvature, triangle anomalies, and the chiral magnetic effect in Fermi liquids. *Phys. Rev. Lett.* **109**, 181602 (2012).
46. M. A. Stephanov, Y. Yin, Chiral kinetic theory. *Phys. Rev. Lett.* **109**, 162001 (2012).
47. J. Y. Chen, D. T. Son, M. A. Stephanov, H. U. Yee, Y. Yin, Lorentz invariance in chiral kinetic theory. *Phys. Rev. Lett.* **113**, 182302 (2014).
48. J. Y. Chen, D. T. Son, M. A. Stephanov, Collisions in chiral kinetic theory. *Phys. Rev. Lett.* **115**, 021601 (2015).
49. N. Yoshikawa, T. Tamaya, K. Tanaka, High-harmonic generation in graphene enhanced by elliptically polarized light excitation. *Science* **356**, 736–738 (2017).
50. R. Moessner, P. Surówka, P. Witkowski, Pulsating flow and boundary layers in viscous electronic hydrodynamics. *Phys. Rev. B* **97**, 161112 (2018).
51. M. Semenyakin, G. Falkovich, Alternating currents and shear waves in viscous electronics. *Phys. Rev. B* **97**, 085127 (2018).
52. H. A. Hafez *et al.*, Extremely efficient terahertz high-harmonic generation in graphene by hot Dirac fermions. *Nature* **561**, 507–511 (2018).
53. R. Moessner, N. Morales-Durán, P. Surówka, P. Witkowski, Boundary-condition and geometry engineering in electronic hydrodynamics. *Phys. Rev. B* **100**, 155115 (2019).
54. P. S. Alekseev, Magnetic resonance in a high-frequency flow of a two-dimensional viscous electron fluid. *Phys. Rev. B* **98**, 165440 (2018).
55. M. Chandra, G. Kataria, D. Sahdev, R. Sundararaman, Hydrodynamic and ballistic AC transport in two-dimensional Fermi liquids. *Phys. Rev. B* **99**, 165409 (2019).
56. A. Levchenko, J. Schmalian, Transport properties of strongly coupled electron–phonon liquids. *Ann. Phys.* **419**, 168218 (2020).

57. J. W. McIver *et al.*, Light-induced anomalous Hall effect in graphene. *Nat. Phys.* **16**, 38–41 (2020).
58. I. Sodemann, L. Fu, Quantum nonlinear Hall effect induced by berry curvature dipole in time-reversal invariant materials. *Phys. Rev. Lett.* **115**, 216806 (2015).
59. T. Morimoto, S. Zhong, J. Orenstein, J. E. Moore, Semiclassical theory of nonlinear magneto-optical responses with applications to topological Dirac/Weyl semimetals. *Phys. Rev. B* **94**, 245121 (2016).
60. A. A. Burkov, Dynamical density response and optical conductivity in topological metals. *Phys. Rev. B* **98**, 165123 (2018).
61. G. B. Osterhoudt *et al.*, Colossal mid-infrared bulk photovoltaic effect in a type-I Weyl semimetal. *Nat. Mater.* **18**, 471–475 (2019).
62. L. E. Golub, E. L. Ivchenko, B. Spivak, Semiclassical theory of the circular photogalvanic effect in gyrotropic systems. *Phys. Rev. B* **102**, 085202 (2020).
63. S. Kovalev *et al.*, Non-perturbative terahertz high-harmonic generation in the three-dimensional Dirac semimetal Cd_3As_2. *Nat. Commun.* **11**, 2451 (2020).
64. B. Cheng *et al.*, Efficient terahertz harmonic generation with coherent acceleration of electrons in the dirac semimetal Cd_3As_2. *Phys. Rev. Lett.* **124**, 117–402 (2020).
65. P. O. Sukhachov, E. V. Gorbar, Stray magnetic field and stability of time-dependent viscous electron flow. *Phys. Rev. B* **104**, 195111 (2021).
66. C. P. Weber, Ultrafast investigation and control of Dirac and Weyl semimetals. *J. Appl. Phys.* **129**, 070901 (2021).
67. R. M. A. Dantas, Z. Wang, P. Surówka, T. Oka, Nonperturbative topological current in Weyl and Dirac semimetals in laser fields. *Phys. Rev. B* **103**, L201105 (2021).
68. D. B. Tanner, *Optical Effects in Solids* (Cambridge University Press, 2019).
69. M. I. Kaganov, G. Y. Lyubarskiy, A. G. Mitina, The theory and history of the anomalous skin effect in normal metals. *Phys. Rep.* **288**, 291–304 (1997).
70. D. T. Son, B. Z. Spivak, Chiral anomaly and classical negative magnetoresistance of Weyl metals. *Phys. Rev. B* **88**, 104412 (2013).
71. B. Z. Spivak, A. V. Andreev, Magnetotransport phenomena related to the chiral anomaly in Weyl semimetals. *Phys. Rev. B* **93**, 085107 (2016).
72. A. A. Burkov, Chiral anomaly and diffusive magnetotransport in Weyl metals. *Phys. Rev. Lett.* **113**, 247203 (2014).
73. P. J. Ledwith, H. Guo, L. Levitov, The hierarchy of excitation lifetimes in two-dimensional fermi gases. *Ann. Phys.* **411**, 167913 (2019).
74. E. I. Kiselev, J. Schmalian, Nonlocal hydrodynamic transport and collective excitations in Dirac fluids. *Phys. Rev. B* **102**, 245434 (2020).
75. H. Guo, E. Ilseven, G. Falkovich, L. S. Levitov, Higher-than-ballistic conduction of viscous electron flows. *Proc. Natl. Acad. Sci. U.S.A.* **114**, 3068–3073 (2017).
76. A. Lucas, Stokes paradox in electronic fermi liquids. *Phys. Rev. B* **95**, 115425 (2017).
77. A. Lucas, S. A. Hartnoll, Kinetic theory of transport for inhomogeneous electron fluids. *Phys. Rev. B* **97**, 045105 (2018).
78. H. Lamb, On electrical motions in a spherical conductor. *Philos. Trans. R. Soc. Lond.* **174**, 519–549 (1883).
79. G. E. H. Reuter, E. H. Sondheimer, The theory of the anomalous skin effect in metals. *Proc. R. Soc. Lond. A Math. Phys. Sci.* **195**, 336–364 (1948).
80. D. Valentinis, Optical signatures of shear collective modes in strongly interacting fermi liquids. *Phys. Rev. Res.* **3**, 023076 (2021).
81. R. N. Gurzhi, Contribution to the theory of the skin effect in metals at low temperatures. *Sov. Phys. JETP* **20**, 1228–1230 (1964).
82. C. Duval, Z. Horváth, P. A. Horváthy, L. Martina, P. C. Stichel, Berry phase correction to electron density in solids and "exotic" dynamics. *Mod. Phys. Lett. B* **20**, 373–378 (2006).
83. A. Knoll, C. Timm, T. Meng, Negative longitudinal magnetoconductance at weak fields in Weyl semimetals. *Phys. Rev. B* **101**, 201402 (2020).
84. C. Xiao *et al.*, Linear magnetoresistance induced by intra-scattering semiclassics of Bloch electrons. *Phys. Rev. B* **101**, 201410 (2020).
85. Y. Gao, S. A. Yang, Q. Niu, Geometrical effects in orbital magnetic susceptibility. *Phys. Rev. B* **91**, 214405 (2015).
86. Y. Gao, S. A. Yang, Q. Niu, Field induced positional shift of Bloch electrons and its dynamical implications. *Phys. Rev. Lett.* **112**, 166601 (2014).
87. E. V. Gorbar, V. A. Miransky, I. A. Shovkovy, P. O. Sukhachov, Second-order chiral kinetic theory: Chiral magnetic and pseudomagnetic waves. *Phys. Rev. B* **95**, 205141 (2017).
88. N. Abbasi, F. Taghinavaz, O. Tavakol, Magneto-transport in a chiral fluid from kinetic theory. *J. High Energy Phys.* **2019**, 51 (2019).
89. S. Z. Yang, J. H. Gao, Z. T. Liang, Q. Wang, Second-order charge currents and stress tensor in a chiral system. *Phys. Rev. D* **102**, 116024 (2020).
90. J. H. Ferziger, H. G. Kaper, *Mathematical Theory of Transport Processes in Gases* (North-Holland, 1972).
91. C. Cercignani, *The Boltzmann Equation and Its Applications* (Springer, 1988).
92. A. Lucas, S. Das Sarma, Electronic sound modes and plasmons in hydrodynamic two-dimensional metals. *Phys. Rev. B* **97**, 115449 (2018).
93. N. Kumar *et al.*, Extremely high magnetoresistance and conductivity in the type-II Weyl semimetals WP_2 and MoP_2. *Nat. Commun.* **8**, 1642 (2017).
94. A. A. Abrikosov, *Fundamentals of the Theory of Metals* (North-Holland, 1988).
95. P. O. Sukhachov, L. I. Glazman, Anomalous electromagnetic field penetration in a Weyl or Dirac semimetal. *arXiv* [Preprint] (2021). https://arxiv.org/abs/2110.10167 (Accessed 25 January 2022).